ACS APPLIED BIO MATERIALS

www.acsabm.org Article

Multifunctional Titanium Surfaces for Orthopedic Implants: Antimicrobial Activity and Enhanced Osseointegration

Fiorela Ghilini, Natalia Fagali, Diego E. Pissinis, Guillermo Benítez, and Patricia L. Schilardi*

Cite This: https://doi.org/10.1021/acsabm.1c00613 Read Online

ACCESS | Metrics & More | Article Recommendations

ABSTRACT: The use of implants in orthopedics and dental practice is a widespread surgical procedure to treat diverse diseases. However, peri-implantitis due to infections and/or poor osseointegration can lead to metallic implant failure. The aim of this study was to develop a multifunctional coating on titanium (Ti) surfaces, to simultaneously deal with both issues, by combining antibacterial silver nanoparticles (AgNPs) and regenerative properties of lactoferrin (Lf). A simple and cost-effective methodology that allows the direct multifunctionalization of Ti surfaces was developed. The modified surfaces were characterized by AFM, X-ray photoelectron spectroscopy, and contact angle measurements. Additionally, *in vitro* preosteoblast cell adhesion, cell viability, and differentiation were evaluated. The antibacterial capability of the surfaces was tested against *Staphylococcus aureus* as a prosthesis infection model strain. Our results showed that Lf adsorbed on both Ti surfaces and Ti surfaces with adsorbed AgNPs. Simultaneously, the presence of Lf and AgNPs notably improved preosteoblast adhesion, proliferation, and differentiation, whereas it reduced the bacterial colonization by 97.7%. Our findings indicate that this simple method may have potential applications in medical devices to both improve osseointegration and reduce bacterial infection risk, enhancing successful implantation and patients' quality of life.

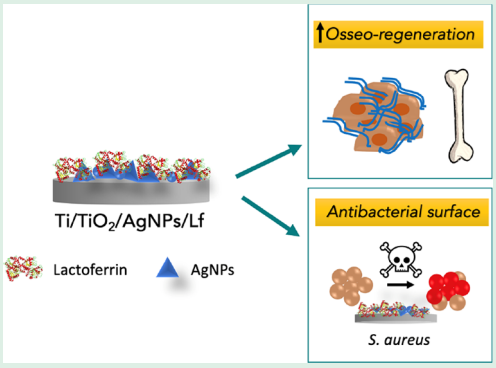

KEYWORDS: *Ti implants, antibacterial, osseointegration, multifunctional surfaces, lactoferrin, silver nanoparticles*

1. INTRODUCTION

The use of implants in orthopedics and dental practice to keep damaged bones in their proper alignment or to replace damaged bones or connective tissue is a widespread surgical practice to treat diverse diseases such as trauma, osteoporosis, bone cancer, and joint and spinal injuries, among others.[1] In 2007, Kurtz *et al.* estimated that at the end of 2030, hip replacement will rise by 174% (572,000 procedures) and the number of total knee arthroplasties will grow by 673% (3.48 million procedures) only in the United States.[2] However, the incidence of implant failures is around 10% and the leading causes are bacterial infections and/or poor osseointegration.[3] The outcomes for the patients include chronic pain, disability, longer healing time, revision surgery, and incremental cost of healthcare. Hence, implant designs need to include both good tissue integration and antibacterial properties, both being essential criteria for a successful implantation.[4] So far, most of the research studies described in the literature have focused only on improving cell adhesion or preventing bacterial infection, but few of them deal with combined effects to overcome both issues at the same time. Thus, multifunctional coatings are emerging as a powerful strategy to develop sophisticated biomaterials with enhanced performance.[3]

To induce the required osseointegration after implantation, appropriate surface conditions must be generated to guarantee optimal cell adhesion, proliferation, and differentiation. This event enables mineral matrix production leading to new bone formation. Titanium (Ti) and its alloys have been extensively used on medical devices due to their mechanical properties, similar to those of bone,[5] and good biocompatibility. Today, Ti implants can be custom-fabricated with the required geometry to match patients' anatomical structure to improve material performance.[6]

Many authors have studied several strategies to increase the osteoblast growth on Ti implants.[7] For instance, Balasundaram *et al.* reported a nanocrystalline hydroxyapatite-coated Ti surface by using molecular plasma deposition, which improved the osteoblast density,[8] and recently, Suo *et al.* developed a graphene oxide/chitosan/hydroxyapatite coating that greatly increased the cell−material interactions *in vitro*.[9] However,

Received: May 26, 2021
Accepted: July 23, 2021

ACS Publications © XXXX American Chemical Society

these works do not consider the bacterial adhesion on implant surfaces. However, the use of antimicrobial and anti-biofouling coatings such as metallic nanoparticles or bioactive molecules, like chitosan and hyaluronic acid, has been widely explored to prevent bacterial adhesion on implants.[10,11] Nevertheless, these coatings result in low osteoblast adhesion and differentiation or even in cytotoxic effects.[12] Thus, blending different therapeutic agents with specific properties can be a promising strategy to deal with this issue. For example, the combination of hyaluronic acid/chitosan multilayers with the cell-adhesive RGD peptide reduced bacterial adhesion on TiO_2, while enhancing the interaction of the materials with osteogenic cells.[13] Another approach consists in the loading of TiO_2 nanotubes, which have shown effective interaction with osteogenic cells,[14] with antimicrobial agents such as silver nanoparticles (AgNPs),[15] chitosan,[16] and antibiotics.[17] All of these systems have successfully achieved the expected results, but these strategies may also have some disadvantages, such as complex fabrication, including several steps or specific equipment; polymers may degrade in the physiological environment; or more importantly, the noncontrolled release of antimicrobials can induce cytotoxicity,[18] lower drug effects, and the persistent bacterial resistance.[19]

Silver (Ag), including nanoparticle, ion, and metal forms, is widely recognized for its antibacterial and antifungal properties and has been used for years in medical treatments[20] Besides, the main advantage of Ag lies in the lack of bacterial resistance. Particularly, AgNP adsorption on Ti has been well-studied as an antimicrobial coating for medical devices.[21,22] It has been proposed that the good antibacterial and antibiofilm properties of adsorbed AgNPs on bulk materials are due to both the continuous and slow release of Ag(I) ions produced in oxygen-containing aqueous media and the direct nanomechanical action of the AgNP surface on the bacterial cell wall, which promote the disruption of the bacterial membrane, leading to cell death.[23]

Lactoferrin (Lf) is an iron (Fe)-binding protein that can be found in mammalian mucosal secretions, such as tears, saliva, colostrum, and milk.[24] This biomolecule is important in the protein-based medicine field since its broad range of protective effects goes from anticancer, anti-inflammatory, and immune modulator activities to antimicrobial activity against a large number of microorganisms. Regarding the Lf antimicrobial activity, several mechanisms have been proposed, including the ability to bind large amounts of Fe(III) inhibiting bacterial growth[25] and the direct interaction with bacterial surfaces, to damage the external membrane of Gram-negative[26] cells, and to bind to anionic molecules (e.g., lipoteichoic acid) of the bacterial cell wall, reducing the negative charge on the Gram-positive bacteria.[25] Additionally, various authors have demonstrated the regenerative properties of Lf on different tissues. Cornish *et al.* showed that at physiological concentrations, Lf strongly stimulates the proliferation and differentiation of primary osteoblasts, while it inhibits osteoclastogenesis.[27] All of these properties together make Lf a promising biodegradable and biocompatible material that could be exploited as an active multifactorial therapeutic agent.[28] Nevertheless, the methodologies involved required surface pretreatment or linker molecules to indirectly attach the protein,[29,30] increasing the complexity of the preparation procedure and costs.

This work aims to develop a multifunctional surface that has an antibacterial effect and also promotes osseoregeneration. To this end, a novel method for the Ti multifunctionalization through the combined adsorption of Lf and AgNPs is presented. A two-step procedure was used to achieve the double functionalization: Ti disks were first immersed in AgNP dispersion for nanoparticle adsorption, followed by immersion in Lf solution to attach the protein molecules. The surfaces were characterized through a multitechnique approach, namely, X-ray photoelectron spectroscopy (XPS), AFM, and contact angle measurements. Since the Ti surface is covered with a native oxide layer,[31] the substrates will hereafter be denoted as Ti/TiO_2. The osseoinductive and antibacterial properties of the resulting surfaces were assessed through preosteoblast adhesion, proliferation, and differentiation studies together with antibacterial bioassays.

2. MATERIALS AND METHODS

2.1. AgNP Synthesis. AgNPs were synthesized, according to Frank *et al.*,[32] by the addition of 2.0 mL of 1.25×10^{-2} M sodium citrate, 5.0 mL of 3.75×10^{-4} M silver nitrate, and 5.0 mL of 5.0×10^{-2} M hydrogen peroxide. The Ag(I) reduction was achieved by adding 2.5 mL of freshly prepared 5.0×10^{-3} M sodium borohydride under vigorous magnetic stirring. The colloidal dispersion was then dialyzed for 2 h to eliminate the excess of reagents. The synthesis leads to citrate-capped polydisperse AgNPs, which have been exhaustively characterized in a previous work of Ghilini *et al.*[22] Two populations were described and consist of nanodisks (12−15 nm in diameter and 7 ± 1 nm in height) and nanoprisms (40 nm in size and 8.3 ± 0.8 nm in height). We have chosen these polydisperse nanoparticles because small nanodisks are appropriate for a high efficacy in silver release, whereas bigger nanoprisms, which showed enhanced antibacterial activity,[33] could also act as a silver reservoir at longer times.

2.2. Lf from Bovine Milk. Lf from bovine milk >85% (M_W: 87 kDa, Sigma-Aldrich, Germany) was characterized by dynamic light scattering (DLS) using Malvern Zetasizer Nano series equipment. For this purpose, Lf was dissolved in phosphate-buffered saline (PBS) solution (pH = 7.4) at a concentration of 1.2 mg/mL and it was diluted at a ratio of 1:4 prior to the size measurement (ionic strength: 162.7 mM).

2.3. Ti/TiO_2 Functionalization with AgNPs and Lf. Ti disks (0.7 cm in diameter, 99.6%, Advent) polished to mirror grade with diamond paste were used as substrates. The substrates were washed with ethanol, rinsed with ultrapure water (Milli-Q), and dried under N_2 stream. Lf-coated substrates were obtained by immersing the samples in the Lf solution for 24 h at 4 °C. After that, the Lf-functionalized Ti disks ($Ti/TiO_2/Lf$) were gently rinsed with ultrapure water. Double functionalization of Ti/TiO_2 disks with AgNPs and Lf was carried out in two steps: first, clean Ti substrates were immersed in AgNP dispersion for 3 h and then rinsed with ultrapure water. After that, the substrates ($Ti/TiO_2/AgNPs$) were immediately covered with 15 μL of the Lf-buffered solution (1.2 mg/mL) and left for 24 h at 4 °C. Finally, the multifunctionalized Ti disks ($Ti/TiO_2/AgNPs/Lf$) were gently rinsed with ultrapure water. Clean Ti/TiO_2 disks, $Ti/TO_2/Lf$, and $Ti/TiO_2/AgNPs$ were used as controls with comparative purposes.

2.4. Physicochemical Characterization of the Modified Substrates. To characterize the functionalized surfaces, topographic AFM images of each sample were acquired in air in Tapping mode using a multimode microscope with a Nanoscope V control unit from Bruker. Scan rates of 0.9−1.2 Hz and RTESP (251−314 kHz and 40 N/m) tips from Bruker were used. Roughness data (R_a) were obtained from three separate images from different regions on each substrate using Nanoscope V Software. R_a was calculated as the arithmetic average of the absolute values of the surface height deviations measured from the mean plane.

The surface chemical composition was analyzed by XPS. Measurements of the substrates were performed using an Al Kα source (XR50, Specs GmbH) and a hemispherical electron energy analyzer (PHOIBOS 100, Specs GmbH) operating at a pass energy of 40 or

https://doi.org/10.1021/acsabm.1c00613
ACS Appl. Bio Mater. XXXX, XXX, XXX−XXX

10 eV for either low-resolution or high-resolution spectra. Two-point calibration of the energy scale was performed using sputter cleaned gold (Au $4f_{7/2}$, binding energy = 84.00 eV) and copper (Cu $2p_{3/2}$, binding energy = 932.67 eV) samples. C 1s at 285 eV was used as a charging reference. The experiments were carried out in duplicate, and the spectral analysis was carried out using CasaXPS v2.3.14 and XPS Peak 4.0 software packages.

The wettability of the samples was determined by the static contact angle measurement using a Ramé-Hart 290 goniometer. Ultrapure water was used as a working fluid. The water drop volume was 2 μL, and the measurements were performed at room temperature in triplicate. Then, data were analyzed using DROPImage software.

2.5. Biological Assays. *2.5.1. Bacterial Culture.* *Staphylococcus aureus* (*S. aureus*, ATCC 25923) was grown overnight in nutrient broth (NB; Merck, Darmstadt, Germany) at 37 °C in vigorous agitation (180 rpm). Optical density measurements of bacterial inoculums were performed by UV−vis spectroscopy at 586 nm, and then, appropriate dilution was made in NB to get ∼10^8 colony-forming units (CFU) mL^{-1} to be used in antimicrobial assays.

2.5.2. Antimicrobial Properties of Modified Ti. The evaluation of the antimicrobial properties of Ti/TiO_2/AgNPs, Ti/TiO_2/Lf, and Ti/TiO_2/AgNPs/Lf substrates was carried out as reported previously,[22] and the Ti/TiO_2 surfaces were used as control. In brief, substrates were placed vertically into each well of a 24-multiwell plate. Then, the wells were fulfilled with the bacterial dilution (∼10^8 CFU mL^{-1}) and incubated at 37 °C for 2 h to form an early biofilm. After that, the substrates were removed from NB and gently washed three times by immersing in sterile water with the aim of removing the cells weakly attached to the surface. Next, the disks were incubated for 24 h at 37 °C in a 24-well culture plate with a rich phosphate-buffered medium containing 5 g/L glucose, 5 g/L mannitol, and 10 g/L glycine in 0.01 M phosphate buffer with a pH of 7 (hereafter denoted as GMP). Finally, the substrates were gently washed, individually placed in glass tubes for sonication, and then quantified by the plate count method. The experiments were made by quadruplicate.

2.5.3. Fluorescence Microscopy. Viability of the *S. aureus* biofilm grown on Ti/TiO_2/AgNPs, Ti/TiO_2/Lf, and Ti/TiO_2/AgNPs/Lf substrates for 24 h was determined by using a LIVE/DEAD Backlight kit (SYTO 9 and propidium iodide, Invitrogen), according to the kit protocol. Ti/TiO_2 surfaces were used as control. Dye (15 μL) was poured onto each substrate and kept in the dark for 15 min at room temperature. Then, the dyed biofilm substrates were gently rinsed with sterile water, and fluorescent bacteria were visualized by fluorescence microscopy with an Olympus BX-51 microscope. UMWG2 (excitation, 510−550 nm; emission, 590 nm) and U-MWB2 (excitation, 460−490 nm; emission, 520 nm) filters were used. Bacteria were kept hydrated for the entire procedure.

2.5.4. Cell Cultures. Mouse preosteoblast cell line MC3T3-E1 and macrophages RAW 264.7 were grown as monolayers in T-25 flasks with Dulbecco's modified Eagle's medium (DMEM) culture medium (GIBCO-BRL, Los Angeles, USA) supplemented with 10% inactivated fetal calf serum (Natocor, Villa Carlos Paz, Córdoba, Argentina), 50 IU/mL penicillin, and 50 μg/mL streptomycin sulfate in a humidified incubator at 37 °C and in a 5% CO_2 atmosphere.

Viable cells were counted in a Neubauer hemocytometer by the exclusion Trypan Blue (Sigma-Aldrich, St. Louis, MO, USA) method.

2.5.5. Preosteoblast and Macrophage Cell Adhesion by Acridine Orange Staining. To compare the efficiency of cell adhesion on the different substrates, preosteoblast cells MC3T3-E1 were seeded at 3.7 × 10^4 cells/cm^2 on each sample. Briefly, 50 μL of culture media containing cells was seeded onto Ti/TiO_2 (control), Ti/TiO_2/Lf, Ti/TiO_2/AgNPs, and Ti/TiO_2/AgNPs/Lf and kept for 30 min at 37 °C to promote cell attachment. After that, fresh media was added until 1 mL. The cells onto the samples were incubated for 24 h at 37 °C and in a 5% CO_2 atmosphere.

Macrophages RAW 264.7 were seeded onto the modified surfaces, and Ti/TiO_2 was used as the control at a density of 7.8 × 10^3 cells/cm^2. The cells onto the samples were incubated for 24 h at 37 °C and in a 5% CO_2 atmosphere.

Incubation was followed by gentle washing twice with PBS. Adherent cells were stained with acridine orange (AO) dye (Sigma-Aldrich, St. Louis, MO, USA) and immediately examined by fluorescence microscopy with appropriate filters. The images were taken with an objective 10×, recorded using the cellSens Software (Olympus, Tokyo, Japan), and analyzed using the free Fiji software. The percentage of attached cells relative to control was calculated according to eq 1, where N_s is the number of fluorescent cells in each substrate and N_c is the number of fluorescent cells onto control substrates. Three independent experiments were performed, and 10 pictures of each sample were taken

$$\text{attached cells (\% of control)} = \frac{N_s}{N_c} \times 100 \quad (1)$$

2.5.6. Cell Viability by LIVE/DEAD Cell Vitality Assay Kit Staining. The viability of preosteoblast cells adhered to each sample was determined using a LIVE/DEAD Cell Vitality Assay kit (L34951, Invitrogen) and fluorescence microscopy according to the manufacturer's protocol. Culture conditions were the same as explained in Section 2.5.5. Death control cells were prepared by incubation of MC3T3-E1 cells adhered to Ti/TiO_2 with 2 mM H_2O_2 under standard cell growth conditions for 24 h.

After the incubation period, all samples were gently washed with sterile PBS twice, followed by dropping 50 μL of staining solution and incubating for 15 min in the dark at 37 °C and in a 5% CO_2 atmosphere. Then, images of stained cells were captured by fluorescence microscopy, and live cell percentage with respect to total adhered cells was calculated for each condition according to eq 2

$$\text{live cells (\% of total cells)} = \frac{\text{red stained area (live cells)}}{\text{total stained area (live + dead cells)}} \times 100 \quad (2)$$

2.5.7. Cell Differentiation Analysis. To promote cell differentiation toward mature osteoblast, MC3T3-E1 cells were incubated with an osteogenic medium prepared as follows: DMEM medium was supplemented with 10 mM β-glycerol phosphate and 50 μg/mL ascorbic acid, which are known as differentiation gene activators.[34] Osteogenic media were renewed for every 3 days.

2.5.7.1. Alkaline Phosphatase Activity by SK-5100 Vector Red Kit Staining. After 15 days of incubation with osteogenic media, cells on the different substrates were gently rinsed with PBS and stained with 50 μL of work solution of Vector Red Alkaline Phosphatase (ALP) Substrate kit. The Vector Red Substrate produces a fluorescent red reaction product in the presence of an ALP enzyme. After 30 min of incubation in darkness, each substrate was rinsed with PBS and immediately observed using a fluorescence microscope with a UMWG2 filter (excitation, 510−550 nm; emission, 590 nm). Ti/TiO_2 surfaces were used as controls. Then, the ALP activity was estimated by percentage of the stained area on each surface, which is as follows:

$$\text{ALP activity (\% stained area)} = \frac{\text{red stained area ALP (sample)}}{\text{total area}} \times 100 \quad (3)$$

2.5.7.2. Type I Collagen Production and Mineralization Determination by Colorimetric Assays. The type I collagen production and mineralization were determined as reported elsewhere.[35] The cells on the different substrates were incubated with osteogenic media for 21 days. After that, the samples were gently rinsed with PBS, fully covered with Bouin solution (the ratio of picric acid, formaldehyde, and acetic acid is 15:5:1), and incubated for 30 min. Then, the samples were rinsed with distilled water and covered with Sirius Red 0.1% p/v (picric acid solution 0.1% p/v) for 1 h. This colorant reacts with amine groups of collagen type I producing a pink complex.[36] Finally, the substrates were washed with 0.01 N HCl solution, and the complex was extracted from cells with 0.1 N NaOH solution. Ti/TiO_2 surfaces were used as controls. Absorbance was

https://doi.org/10.1021/acsabm.1c00613
ACS Appl. Bio Mater. XXXX, XXX, XXX−XXX

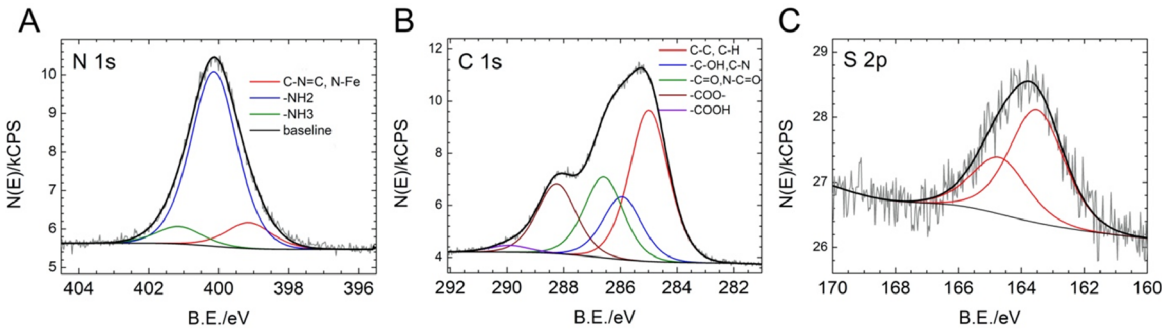

Figure 1. XPS spectra and peak fitting for Ti/TiO_2/Lf samples: (A) N 1s, (B) C 1s, and (C) S 2p.

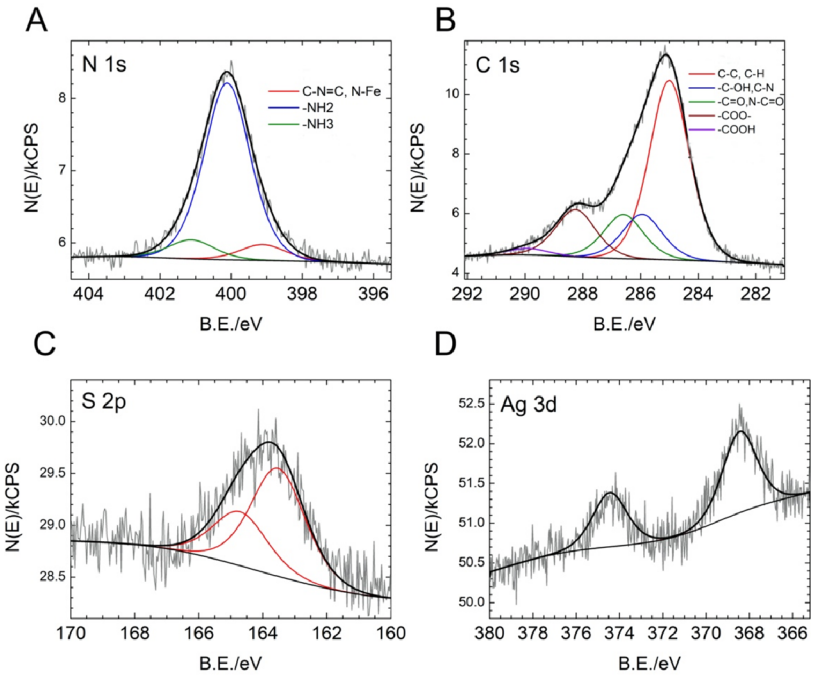

Figure 2. XPS spectra and peak fitting for Ti/TiO_2/AgNPs/Lf samples: (A) N 1s, (B) C 1s, (C) S 2p, and (D) Ag 3d.

read at λ = 550 nm, and the collagen production was expressed as a percentage of control, as given in eq 4

$$\text{type I collagen (\% of control)} = \frac{\text{Abs}_{550}\ \text{sample}}{\text{Abs}_{550}\ \text{control}} \times 100 \quad (4)$$

Mineralization grade was determined by quantifying Ca(II) deposition based on the Alizarin Red staining protocol. This dye selectively attaches to Ca(II) at pH 4.2, forming a red-orange solid soluble at an alkaline pH.[37] Cells attached to each surface were incubated for 21 days in an osteogenic medium, and after that period, the cells were washed with PBS. The cells were fixed with 10% formalin in phosphate buffer (pH 7.1) for 10 min and immediately rinsed with distilled water. After that, substrates were covered with alizarin aqueous solution (2% p/v, pH 4.2) for 10 min. Then, the dye was removed and washed thrice with distilled water, and the precipitate was solubilized with 0.1 N NaOH solution. Ti/TiO_2 surfaces were used as controls. Finally, the absorbance of the solution was measured at λ = 548 nm to calculate mineralization as a percentage of control, as given in eq 5.

$$\text{mineralization (\% of control)} = \frac{\text{Abs}_{548}\ \text{sample}}{\text{Abs}_{548}\ \text{control}} \times 100 \quad (5)$$

2.5.8. Statistical Analysis. Statistical differences were analyzed using ANOVA plus the multiple range test of Bonferroni.[38] All of the measurements were presented as the mean ± standard error of the mean. Differences were considered statistically significant at $p < 0.05$.

3. RESULTS AND DISCUSSION

3.1. Surface Characterization. The AgNP and Lf adsorption on Ti/TiO_2 was analyzed by a multitechnique approach, namely, XPS, AFM, and contact angle measurements. It is well-known that in an oxygen-rich or aqueous atmosphere and at room temperature, the Ti surface is covered by a native oxide layer exposing −OH functional groups, which makes the surface more hydrophilic. Also, the isoelectric point of Ti/TiO_2 is 5−5.5, resulting in a negatively charged surface at physiological pH. These physicochemical features of the surface promote the protein[39] and citrate-coated AgNP adsorption,[10] as it was previously reported.

XPS spectra were acquired for N, C, and S for both Ti/TiO_2/Lf (Figure 1) and Ti/TiO_2/AgNPs/Lf (Figure 2), for which the Ag spectrum was also recorded. The N 1s signal shows three contributions, corresponding to NH−C═O/C−NH_2, NH_3^+, and C−N═C/N−Fe groups (Figures 1A and 2A), which are typical for organic nitrogen species, at 400, ≈402, and ≈399.2 eV, respectively. The C 1s high-resolution spectra reveal five main transitions at 285 (adventitious

https://doi.org/10.1021/acsabm.1c00613
ACS Appl. Bio Mater. XXXX, XXX, XXX−XXX

carbon/C−H/C−C), 285.95, 286.6, 288.25, and 290 eV assigned to C−H/C−C, C−OH/C−N, −C═O/N−C═O, −COO−, and COOH, respectively (Figures 1B and 2B).

These results confirm the presence of protein on both substrates. The COOH and COO^- signal can be attributed to both the Lf amino acids and the citrate capping of AgNPs.[10] The S 2p spectrum can be fitted with a doublet at 163.5 eV, corresponding to C−S−S−C moieties of the protein's third structure (Figures 1C and 2C). Importantly, the signal expected at 161 eV for S−Ag bonds[40] is not observed (Figure 2C), suggesting that if Lf interacts with AgNPs, this is produced by electrostatic interactions between negatively charged AgNPs and the Ti/TiO_2 surface and positive Lf. Figure 2D shows the Ag 3d spectrum for Ti/TiO_2/AgNPs/Lf substrates with the typical double peak at 368.3 eV, attributed to Ag^0.[41] It has been previously reported that electrostatic interactions are responsible for the Lf adsorption on Ti surfaces, in agreement with our results.[42]

The wetting properties of biocompatible surfaces are important for cell attachment, which will promote tissue formation and growth on implants. Some permanent prostheses need to be strongly anchored to the tissue to achieve their mechanical and biological roles,[43] and thus, materials having hydrophilic surfaces are preferred. Hence, the surface hydrophilicity is a significant parameter that should favor osteoblast adhesion without promoting bacterial biofilm formation.[44] The effects of the Ti/TiO_2 functionalization on the surface wettability were monitored by contact angle measurements. The values shown in Table 1 indicate that after the Lf incorporation into the Ti/TiO_2 surface, a reduction in the contact angle is noted, which is consistent with an increase in the surface hydrophilicity.[43,45] Also, the multifunctionalized Ti/TiO_2/AgNPs/Lf samples have the lowest contact angle, indicating a synergic effect when both Lf and AgNPs are present on Ti surfaces. In fact, it has been reported that AgNPs deposited on different surfaces such as polyethylene, hydroxyapatite (dental enamel), and Ti[43] as well as on poly(vinylidene fluoride) membranes[46] decrease the contact angle in relation to that corresponding to the bare substrate. This increased hydrophilicity was attributed to the AgNP oxidation in air-saturated aqueous media,[47] which generates Ag(I) ions, leading to hydrated Ag(I) ions adsorbed on the nanoparticle surface. These hydrated Ag(I) ions were proposed as responsible for the decrease in the contact angle for AgNP-modified surfaces.[46]

Table 1. Contact Angle Values for Bare and Modified Ti/TiO_2*

Ti/TiO_2	Ti/TiO_2/AgNPs	Ti/TiO_2/Lf	Ti/TiO_2/AgNPs/Lf
69.3 ± 4.7[a]	57.8 ± 1.5[b]	45.8 ± 2.8[c]	24.9 ± 1.6[d]

*The values are presented as the mean ± standard deviation of three independent measurements. Different letters mean statistically significant differences ($p < 0.05$).

The surface appearance of the modified samples and Ti/TiO_2 control was analyzed by AFM (Figure 3).

Figure 3B shows the Ti/TiO_2/Lf surface, where bumps with the height ranging between 8 and 5 nm (inset in Figure 3B) can be attributed to Lf on the surface. The bump height well agrees with the Lf size (8 ± 1 nm) obtained by DLS measurements of the protein in aqueous solution and is consistent with the bilobal globular shape with approximate dimensions of 4.0 nm × 5.1 nm × 7.1 nm reported for Lf.[48,49] These bumps are also observed on Ti/TiO_2/AgNPs/Lf surfaces (Figure 3D), where both AgNPs (triangular nanoprisms, red line) and Lf (green line) are individually adsorbed.

The surface roughness was determined by measuring R_a from 2 × 2 μm^2 AFM images (Table 2). The results show the highest R_a values for the multifunctionalized substrate.

3.2. Antibacterial Behavior of Multifunctionalized Surfaces. The ability of the modified surfaces to inhibit the *S. aureus* growth and proliferation was tested. We have chosen *S. aureus* as a model strain because among the surgical site infections (SSI) caused by bacteria, *S. aureus* has been identified as the most reported pathogen. Moreover, from incidence studies, orthopedic procedures lie second in the SSI rate (15.1%),[50] which is a serious issue, considering that SSIs associated with implants may not be evident until 1 year after the procedure. Hence, the experimental model used in this work consisted of the following two steps: (1) bacterial surface colonization in nutritive broth (early biofilm formation), indicated as $t = 0$, and (2) bacterial growth and proliferation on the surface in sterile GMP medium for 24 h, indicated as $t = 24$ (see Section 2). Then, viable cells from the surface were quantified by a serial dilution method after each step.

All of the functionalized Ti/TiO_2 surfaces sowed a killing effect at the initial time ($t = 0$), as the number of viable cells on functionalized surfaces is lower than those found on unmodified substrates (Figure 4, up). Also, bacterial proliferation was inhibited (98.3% for Ti/TiO_2/Lf, 97.6% for Ti/TiO_2/AgNPs, and 97.7% for Ti/TiO_2/AgNPs/Lf) after 24 h of incubation, showing bacteriostatic properties for all of the modified samples. However, epifluorescence microscopy images of the samples after 24 h of incubation (Figure 4, down) show few adhered bacteria on functionalized surfaces, with some of them remaining alive, in good agreement with the quantitative plate counting (Figure 4, up). However, there were no significant differences in the counted CFU for Ti/TiO_2/Lf, Ti/TiO_2/AgNPs, and Ti/TiO_2/AgNPs/Lf, indicating that the multifunctionalization does not lead to a synergic or additive effect.

3.3. Biocompatibility Assays. Initial osteoblast adhesion on the implant surface is crucial for long-term stability and cell differentiation. Furthermore, the ability of cells to adhere on surfaces is influenced by the surface pretreatment, which affects the cell proliferation capacity.[51] However, following initial blood interaction with a foreign body, serum proteins adsorb onto the surface, modulating the immune system response. Consequently, Ti implants may be recognized as foreign bodies and therefore covered by granular and fibrous tissue through a process known as encapsulation,[51] which hinders the proper fixing and integration of the implant. In this context, neutrophils, lymphocytes, monocytes, and finally macrophages play a crucial role in recognizing material surface characteristics and expressing biological factors in the surrounding tissue.[51] Thus, limiting macrophage adhesion and inducing adherent macrophage apoptosis would lead to reduced inflammatory activity and prevent failure of implanted biomedical devices.[51] Consequently, to analyze the cytocompatibility of the functionalized surfaces, the adhesion and viability of MC3T3-E1 preosteoblast cells and Raw 264.7 macrophages were studied.

3.3.1. Preosteoblast Adhesion and Viability. Figure 5 shows the results obtained for the MC3T3-E1 adhesion and survival on the modified surfaces. The cell adhesion is

https://doi.org/10.1021/acsabm.1c00613
ACS Appl. Bio Mater. XXXX, XXX, XXX−XXX

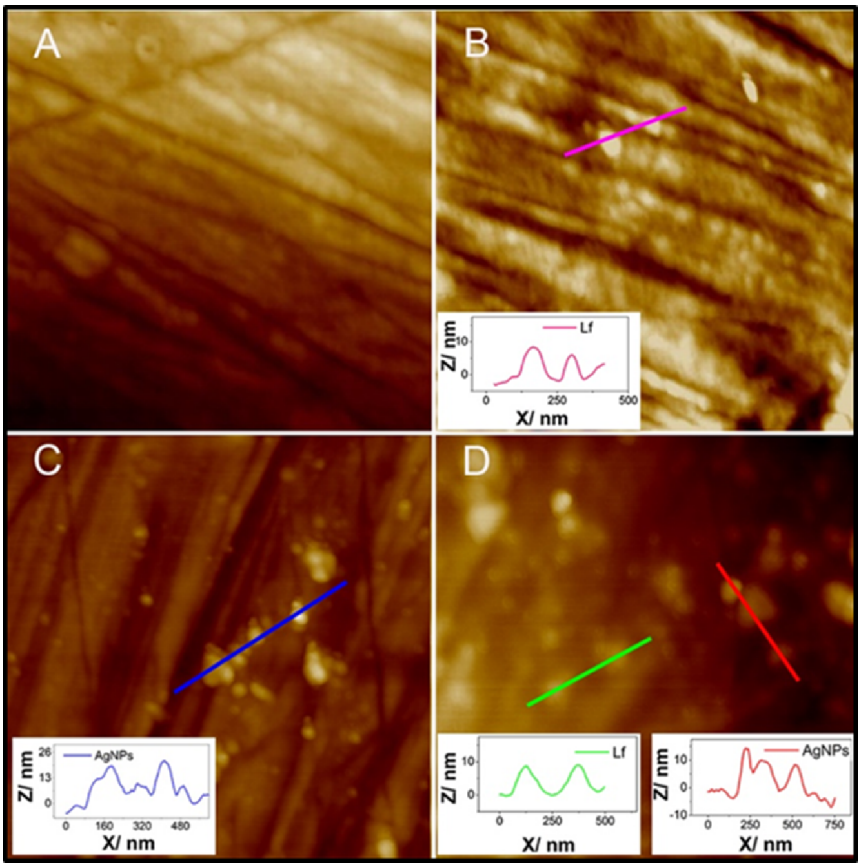

Figure 3. AFM images of (A) Ti/TiO_2 (2×2 μm^2), (B) $Ti/TiO_2/Lf$ (1.5×1.5 μm^2), (C) $Ti/TiO_2/AgNPs$ (2×2 μm^2), and (D) $Ti/TiO_2/AgNPs/Lf$ (1.5×1.5 μm^2). The insets show the cross-sectional analysis along the respective lines.

Table 2. R_a Values for Different Substrates from AFM Images

substrate	average R_a (nm)	SD
Ti/TiO_2	1.6	0.9
$Ti/TiO_2/AgNPs$	2.4	0.1
$Ti/TiO_2/Lf$	2.2	0.6
$Ti/TiO_2/AgNPs/Lf$	7.2*	0.5

*Statistically significant difference ($p \leq 0.05$).

enhanced on $Ti/TiO_2/AgNPs/Lf$ (Figure 5a,b), since the number of cells is 80% higher than the control, whereas the AgNPs or Lf individually adsorbed does not influence the attachment of the cells. These results are also evident in the fluorescence microscopy images of cells stained with AO presented in Figure 5a, where cell confluence (white arrows in Figure 5) can be observed in the multifunctionalized substrate (white arrows in Figure 5b,D), indicating a suitable surface–cell interaction. In addition, the viability of the attached cells was studied using a LIVE/DEAD kit for mammalian cells (Figure 5c), revealing that all cells remained viable after 24 h from adhesion. Therefore, it can be assumed that the modified Ti/TiO_2 surfaces not only are noncytotoxic in the conditions used in this work, but also the combined immobilization of Lf and AgNPs on Ti/TiO_2 leads to a surface that promotes osteoblast cell adhesion. The enhanced cell adhesion can be interpreted in terms of the higher hydrophilicity and higher roughness of the $Ti/TiO_2/AgNPs/Lf$ samples (Tables 1 and 2). The influence of the surface properties on cell adhesion and proliferation has been extensively studied.[52] Regarding the effect of the surface wettability, the general agreement indicates that cells more probably adhere to hydrophilic surfaces than hydrophobic ones. For example, Wei *et al.*[53] analyzed the cell attachment on surfaces having contact angles varying from 0° to 106° and concluded that more fibroblasts adhere as the hydrophilicity of the surface increases. Zelzer *et al.*[54] applied a surface chemical gradient and demonstrated that fibroblasts adhered and proliferated preferentially in the hydrophilic area, showing a gradual decrease in the cell density toward the hydrophobic zone of the gradient. Also, Lim *et al.* found that osteoblast attachment efficiency increases with substratum hydrophilicity.[55] It has been proposed that the surface wettability influences the type, conformation, and binding strength of the proteins adsorbed from culture media, as well as the spatial conformation of extracellular matrix molecules, which mediate the cell adhesion.[56] However, the cell adhesion is also influenced by the surface nanoscale roughness because the nanometer features are considered close to the morphology of natural tissue, thus positively influencing cell adhesion, growth, and maturation. For instance, the increase in the nanoroughness of the biomaterial surface enhances the human venous endothelial cells.[56] In particular, Zareidoost *et al.* analyzed the osteoblast adhesion on Ti surfaces having different roughnesses and found a higher cell attachment on rougher substrates and, therefore, a higher biocompatibility of the Ti surface. Since surface nanoscale roughness approaches to the size of proteins and cell membrane receptors, it could take part in osteoblast differentiation and tissue regeneration.[57]

Lf biocompatibility is well-known for either forming composites[58] or immobilizing on different surfaces.[29,59,60]

https://doi.org/10.1021/acsabm.1c00613
ACS Appl. Bio Mater. XXXX, XXX, XXX−XXX

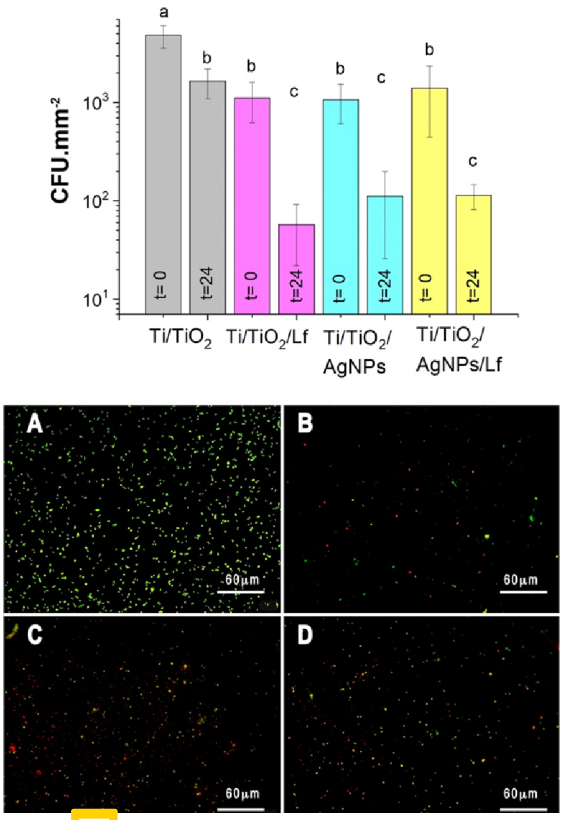

Figure 4. (Top) Attached viable bacteria expressed as CFU mm^{-2} on Ti/TiO$_2$ control and functionalized surfaces at t = 0 and 24 h, on a logarithmic scale. Different letters mean statistically significant differences with $p < 0.05$. (Bottom) Live/Dead BacLight staining after 24 h on Ti/TiO$_2$ (A), Ti/TiO$_2$/Lf (B), Ti/TiO$_2$/AgNPs (C), and Ti/TiO$_2$/AgNPs/Lf (D), with a magnification of 40×. Orange-red: dead cells; green: live cells.

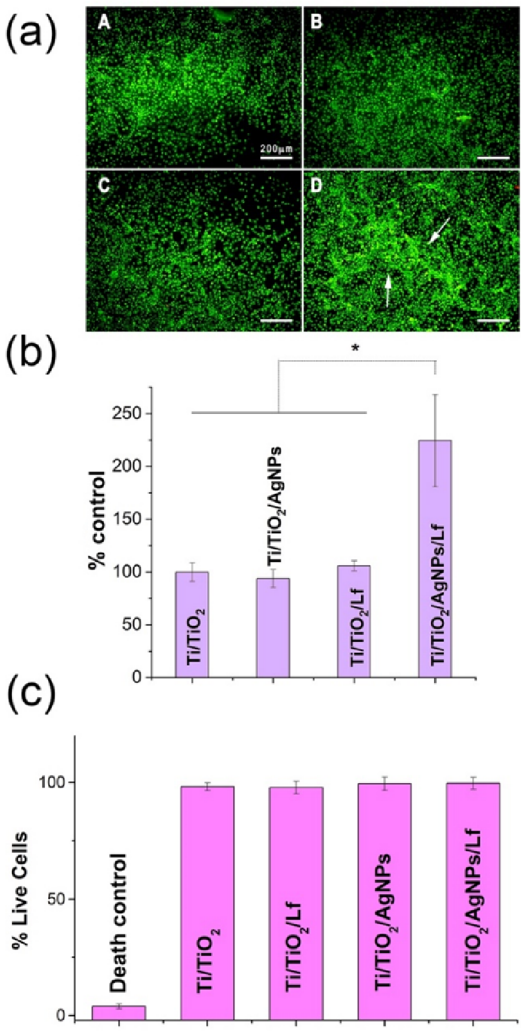

Figure 5. (a) Epifluorescence images of attached preosteoblast cells stained with AO after 24 h of incubation on Ti/TiO$_2$ (A), Ti/TiO$_2$/AgNPs (B), Ti/TiO$_2$/Lf (C), and Ti/TiO$_2$/AgNPs−Lf (D). (b) Number of adhered MC3T3-E1 cells on the different substrates after 24 h of incubation. The results are expressed as % of the control (bare Ti/TiO$_2$). Asterisk means the statistically significant difference ($p < 0.05$). (c) Viable cells (Live/Dead Cell Vitality Assay Kit staining) after 24 h, expressed as % of the total number of adhered cells on each surface. Death control corresponds to H_2O_2-treated cells.

Particularly, Kim *et al.* have studied MG-63 cell adhesion and proliferation onto heparin-dopamine-Lf-modified Ti surfaces, showing that proliferation increases with time in both bare Ti and treated surfaces.[29] However, the biocompatibility, genotoxicity, and cytotoxicity of AgNPs depend on many factors, such as size, shape, surface charge, capping, and concentration, among others. The cellular response to AgNPs differs according to the cell type and the physicochemical nature of the nanoparticles.[61] Most of these studies have been carried out by adding different doses of dispersed AgNPs to the cell culture, but few of them involve adsorbed nanoparticles. Generally speaking, AgNPs at low concentrations have no cytotoxic effects.[62] Hence, our results suggest that the Ti/TiO$_2$/AgNPs/Lf substrates have a suitable antibacterial effect combined with an enhanced promoting effect on preosteoblast adhesion as a result of the influence of both the adsorbed protein and AgNPs.

3.3.2. Macrophage Adhesion. The host response to a foreign body is primarily mediated by macrophages. The acuteness of the reaction depends on the nature of the implanted material, the characteristics of the implant surface, and the individual reaction of the host. The immune response to indwelling devices involves the protein adsorption on the surface, macrophage adhesion and activation, and the release of chemokines that recruit additional macrophages and other immune cells, inducing severe inflammation and leading to chronic inflammation, followed by fusion of macrophages, formation of foreign body giant cells, and finally, the fibrous encapsulation of the implanted material.[63] Thus, the extent of the macrophages' adhesion on the modified substrates was studied and compared with that corresponding to the Ti/TiO$_2$ control. Figure 6a shows epifluorescence images of RAW 264.7 cells stained with AO on the assayed substrates. It can be observed that the cells exhibit a low spreading morphology and conserved their native spherical shape, which could be related to a low macrophage activation.[64] From quantitative analysis (Figure 6b), it can be concluded that the adsorption of Lf, AgNPs, or both AgNPs and Lf does not induce a higher macrophage adhesion nor an enhanced activated phenotype when compared to bare Ti/TiO$_2$. Thus, it is expected that the modified substrates would not trigger an exacerbated immune response. Furthermore, the fact that the multifunctionalized surface enhances the preosteoblast adhesion but does not affect the macrophage attachment would indicate that the surface

https://doi.org/10.1021/acsabm.1c00613
ACS Appl. Bio Mater. XXXX, XXX, XXX−XXX

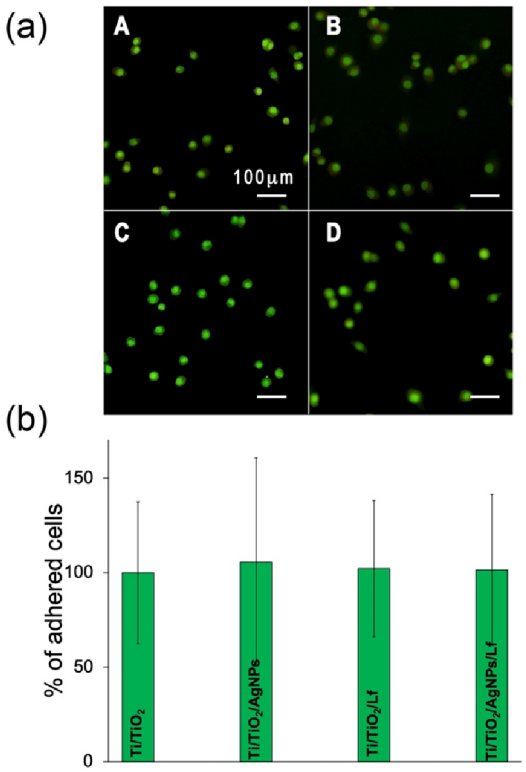

Figure 6. (a) AO-stained macrophages after 24 h of adhesion on (A) Ti/TiO_2, (B) Ti/TiO_2/AgNPs, (C) Ti/TiO_2/Lf, and (D) Ti/TiO_2/AgNPs/Lf. (b) Number of adhered macrophage cells on each surface expressed as % of the control (bare Ti/TiO_2). Cells from 10 images were counted for each substrate.

modification is able to induce selective osteogenesis. Additional investigation is needed to confirm this hypothesis.

3.4. Osseoregenerative Properties of Multifunctionalized Surfaces. Osseoregeneration is important to those orthopedic implants (dental, femoral, and hip) that need to be integrated to the bone to accomplish the intended function. Consequently, promoting the proper adhesion, proliferation, and differentiation of tissue cells is desirable to help the production of the mineralized matrix and bone formation. Lf has the ability to promote osteoblast cell proliferation, differentiation, and mineralization, which is considered as an osteogenic molecule. Moreover, Lf acts as a survival factor in osteoblasts, decreasing apoptosis. Thus, the use of Lf on multicomponent coatings acts as an osteogenic mediator and stimulator, modulating bone fixation to implants.

The collagen extracellular matrix and ALP, which are involved in matrix calcification and osteocyte maturation, are indicators of the new bone tissue formation.[34] Also, the quantification of Ca(II) and PO_4^{-3} ions is used as a marker for osteoblast differentiation since approximately 60% of bone tissue is composed of hydroxyapatite. Thus, the mineralization and differentiation of preosteoblastic MC3T3-E1 cells adhered to the modified surfaces were evaluated through type I collagen, ALP, and Ca(II) ion production.[65]

3.4.1. Collagen and Matrix Mineralization Analysis. Mineralization grade was studied by quantifying Ca(II) and type I collagen production by MC3T3-E1 cells after 21 days of growth on each substrate with osteogenic medium. Higher Ca(II) and collagen concentrations indicate higher differentiation from preosteoblast to mature osteoblast.[65] The results depicted in Figure 7 indicate that Lf or AgNPs adsorbed on the substrates rise the produced Ca(II) levels, but not the

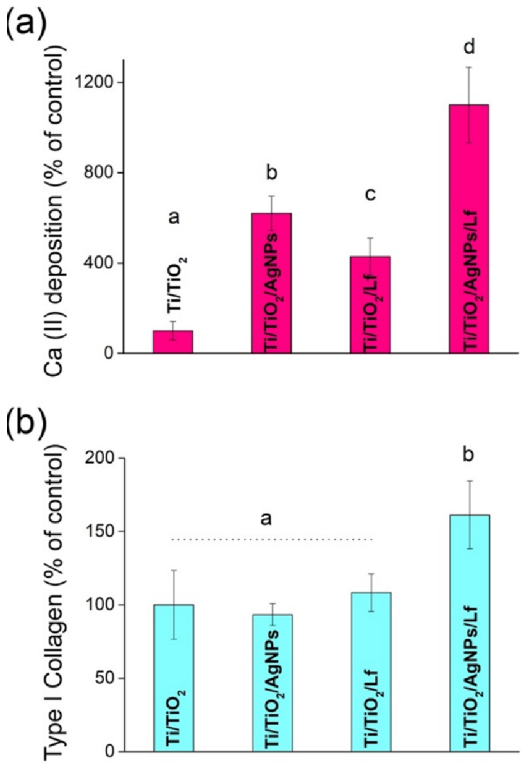

Figure 7. (a) Mineralization grade assessed by the Ca(II) deposition measurement and (b) type I collagen production by MC3T3-E1 cells on each substrate. The results are expressed as % of the control (bare TiO_2). Measurements were carried out after 21 days of incubation in the osteogenic medium. Different letters mean the statistically significant difference, $p < 0.05$.

collagen production, in comparison to the unmodified substrate. However, the simultaneous presence of AgNPs and Lf significantly enhances the amount of both collagen and Ca(II), in concordance with the higher number of adhered preosteoblast cells. Similar outcomes were found in previous reports with Lf-heparin- or Lf-hydroxyapatite-modified surfaces.[66−68]

3.4.2. ALP Analysis. To evaluate the early differentiation of preosteoblast grown onto different substrates *in vitro*, semi-quantitative evaluation of ALP enzyme production after 15 days of incubation was carried out by fluorescence SK-5100 Vector Red kit assay. Our results indicate that the ALP activity was noticeably enhanced by cells exposed to all of the functionalized surfaces compared with Ti/TiO_2 control (Table 3). Besides, Ti/TiO_2/AgNPs/Lf substrates presented the

Table 3. ALP Enzyme Activity Expressed as % of Stained Area in Relation to the Total Area of the Substrate after 15 Days of Incubation in the Osteogenic Medium*

substrate	Ti/TiO_2	Ti/TiO_2/AgNPs	Ti/TiO_2/Lf	Ti/TiO_2/AgNPs/Lf
% stained area	26.4 ± 3.1[a]	43.2 ± 2.0[b]	32.6 ± 6.2[c]	48.5 ± 4.1[b]

*Different letters mean the statistically significant difference ($p < 0.05$).

https://doi.org/10.1021/acsabm.1c00613
ACS Appl. Bio Mater. XXXX, XXX, XXX−XXX

highest levels among all samples (48.5 ± 4.1%). Therefore, the multifunctionalized surface is able to stimulate osseoregeneration.

The higher collagen production, Ca(II) deposition, and ALP activity produced by MC3T3-E1 cells grown on the Ti/TiO_2/AgNP/Lf surface can be attributed to the greater number of preosteoblast cells attached to this surface, which can be explained by its highest hydrophilicity and nanoscale roughness (see Section 3.3.1). Moreover, it has been reported that nanostructured surfaces induce an increase in ALP synthesis and an increased Ca-containing mineral production associated with a higher osteoblast proliferation.[69]

4. CONCLUSIONS

The surface multifunctionalization of Ti with Lf and AgNPs was successfully achieved by a simple two-step protocol.

Our results suggest that the protein molecules adsorb by electrostatic interactions between the positively charged Lf and the negatively charged Ti/TiO_2 and AgNPs. The simultaneous presence of Lf and AgNPs enhances the hydrophilicity and nanoroughness of the substrate, making it suitable for preosteoblast cell adhesion but not for macrophages. The designed surfaces have good antibacterial properties, necessary to inhibit initial bacterial attachment to implants. Although the multifunctionalization does not lead to the synergic or additive antibacterial effect, the blending of AgNPs and Lf on the surface provides an appropriate cytocompatibility and enhances the osteogenic properties, while macrophage attachment is not affected by the modified surface. These results are remarkable clues that the multifunctionalized surface would have an osseointegration-promoting effect without stimulating exacerbated inflammatory or fibrous reaction.

The findings of this work suggest that the multifunctionalized Ti surface is an achievable and promising strategy to reduce prosthesis-related infections and improve the long-term efficacy and stability of implants. The procedure is easy and cost-effective and does not require specific expensive equipment or complex methodologies nor qualified personnel. Importantly, several different implants can be modified simultaneously in each batch. Further studies in this direction should include *in vivo* assays to understand the more realistic behavior of the modified surfaces.

■ AUTHOR INFORMATION

Corresponding Author

Patricia L. Schilardi − *Instituto de Investigaciones Fisicoquímicas Teóricas y Aplicadas (INIFTA), Facultad de Ciencias Exactas, UNLP − CONICET, 1900 La Plata, Buenos Aires, Argentina;* orcid.org/0000-0003-1704-2867; Phone: +54-221-4257430; Email: pls@inifta.unlp.edu.ar; Fax: +54-221-4254642

Authors

Fiorela Ghilini − *Instituto de Investigaciones Fisicoquímicas Teóricas y Aplicadas (INIFTA), Facultad de Ciencias Exactas, UNLP − CONICET, 1900 La Plata, Buenos Aires, Argentina;* orcid.org/0000-0002-4764-7421

Natalia Fagali − *Instituto de Investigaciones Fisicoquímicas Teóricas y Aplicadas (INIFTA), Facultad de Ciencias Exactas, UNLP − CONICET, 1900 La Plata, Buenos Aires, Argentina*

Diego E. Pissinis − *Instituto de Investigaciones Fisicoquímicas Teóricas y Aplicadas (INIFTA), Facultad de Ciencias Exactas, UNLP − CONICET, 1900 La Plata, Buenos Aires, Argentina*

Guillermo Benítez − *Instituto de Investigaciones Fisicoquímicas Teóricas y Aplicadas (INIFTA), Facultad de Ciencias Exactas, UNLP − CONICET, 1900 La Plata, Buenos Aires, Argentina*

Complete contact information is available at: https://pubs.acs.org/10.1021/acsabm.1c00613

Notes

The authors declare no competing financial interest.

This paper is dedicated to the memory of our wonderful colleague Dr. Diego E. Pissinis.

■ ACKNOWLEDGMENTS

The authors gratefully acknowledge CONICET (PIP 112-201501-00601CO), UNLP (Project no. 11/X858), and ANPCyT (PICT-2016-0679, PICT-2016-1424, PICT 2016-2154, and PICT-2020-0034). They also thank Dr. Juan Manuel Fernandez and Dr. María Laura Lastra for their excellent technical assistance in the differentiation experiments.

■ REFERENCES

(1) Lin, X.; Yang, S.; Lai, K.; Yang, H.; Webster, T. J.; Yang, L. Orthopedic Implant Biomaterials with Both Osteogenic and Anti-Infection Capacities and Associated in Vivo Evaluation Methods. *Nanomed. Nanotechnol., Biol. Med.* **2017**, *13*, 123−142.

(2) Kurtz, S.; Ong, K.; Lau, E.; Mowat, F.; Halpern, M. Projections of Primary and Revision Hip and Knee Arthroplasty in the United States from 2005 to 2030. *J. Bone Jt. Surg. - Ser. A* **2007**, *89*, 780−785.

(3) Raphel, J.; Holodniy, M.; Goodman, S. B.; Heilshorn, S. C. Multifunctional Coatings to Simultaneously Promote Osseointegration and Prevent Infection of Orthopaedic Implants. *Biomaterials* **2016**, *84*, 301−314.

(4) Zhao, L.; Chu, P. K.; Zhang, Y.; Wu, Z. Antibacterial Coatings on Titanium Implants. *J. Biomed. Mater. Res., Part B* **2009**, *91B*, 470−480.

(5) Li, J.; Cui, X.; Hooper, G. J.; Lim, K. S.; Woodfield, T. B. F. Rational Design, Bio-Functionalization and Biological Performance of Hybrid Additive Manufactured Titanium Implants for Orthopaedic Applications: A Review. *J. Mech. Behav. Biomed. Mater.* **2020**, *105*, No. 103671.

(6) Pobloth, A. M.; Checa, S.; Razi, H.; Petersen, A.; Weaver, J. C.; Chmidt-Bleek, K.; Windolf, M.; Tatai, A. A.; Roth, C. P.; Schaser, K. D.; Duda, G. N.; Schwabe, P. Mechanobiologically Optimized 3D Titanium-Mesh Scaffolds Enhance Bone Regeneration in Critical Segmental Defects in Sheep. *Sci. Transl. Med.* **2018**, *10*, No. 8828.

(7) Gorgin Karaji, Z.; Jahanmard, F.; Mirzaei, A. H.; Van Der Wal, B.; Amin Yavari, S. A Multifunctional Silk Coating on Additively Manufactured Porous Titanium to Prevent Implant-Associated Infection and Stimulate Bone Regeneration. *Biomed. Mater.* **2020**, *15*, No. 065016.

(8) Balasundaram, G.; Storey, D. M.; Webster, T. J. Molecular Plasma Deposition: Biologically Inspired Nanohydroxyapatite Coatings on Anodized Nanotubular Titanium for Improving Osteoblast Density. *Int. J. Nanomed.* **2015**, *10*, 527−535.

(9) Suo, L.; Jiang, N.; Wang, Y.; Wang, P.; Chen, J.; Pei, X.; Wang, J.; Wan, Q. The Enhancement of Osseointegration Using a Graphene Oxide/Chitosan/Hydroxyapatite Composite Coating on Titanium Fabricated by Electrophoretic Deposition. *J. Biomed. Mater. Res., Part B* **2019**, *107*, 635−645.

(10) Flores, C. Y.; Diaz, C.; Rubert, A.; Benítez, G. A.; Moreno, M. S.; Fernández Lorenzo De Mele, M. A.; Salvarezza, R. C.; Schilardi, P. L.; Vericat, C. Spontaneous Adsorption of Silver Nanoparticles on Ti/TiO2 Surfaces. Antibacterial Effect on Pseudomonas Aeruginosa. *J. Colloid Interface Sci.* **2010**, *350*, 402−408.

(11) Govindharajulu, J. P.; Chen, X.; Li, Y.; Rodriguez-Cabello, J. C.; Battacharya, M.; Aparicio, C. Chitosan-Recombinamer Layer-by-Layer Coatings for Multifunctional Implants. *Int. J. Mol. Sci.* **2017**, *18*, 1−16.

(12) Ferraris, S.; Spriano, S. Antibacterial Titanium Surfaces for Medical Implants. *Mater. Sci. Eng., C* **2016**, *61*, 965−978.

(13) Chua, P. H.; Neoh, K. G.; Kang, E. T.; Wang, W. Surface Functionalization of Titanium with Hyaluronic Acid/Chitosan Polyelectrolyte Multilayers and RGD for Promoting Osteoblast Functions and Inhibiting Bacterial Adhesion. *Biomaterials* **2008**, *29*, 1412−1421.

(14) Lavenus, S.; Trichet, V.; Le Chevalier, S.; Hoornaert, A.; Louarn, G.; Layrolle, P. Cell Differentiation and Osseointegration Influenced by Nanoscale Anodized Titanium Surfaces. *Nanomedicine* **2012**, *7*, 967−980.

(15) Zhao, L.; Wang, H.; Huo, K.; Cui, L.; Zhang, W.; Ni, H.; Zhang, Y.; Wu, Z.; Chu, P. K. Antibacterial Nano-Structured Titania Coating Incorporated with Silver Nanoparticles. *Biomaterials* **2011**, *32*, 5706−5716.

(16) Kumeria, T.; Mon, H.; Aw, M. S.; Gulati, K.; Santos, A.; Griesser, H. J.; Losic, D. Advanced Biopolymer-Coated Drug-Releasing Titania Nanotubes (TNTs) Implants with Simultaneously Enhanced Osteoblast Adhesion and Antibacterial Properties. *Colloids Surf., B* **2015**, *130*, 255−263.

(17) Popat, K. C.; Eltgroth, M.; LaTempa, T. J.; Grimes, C. A.; Desai, T. A. Decreased Staphylococcus Epidermis Adhesion and Increased Osteoblast Functionality on Antibiotic-Loaded Titania Nanotubes. *Biomaterials* **2007**, *28*, 4880−4888.

(18) Duewelhenke, N.; Krut, O.; Eysel, P. Influence on Mitochondria and Cytotoxicity of Different Antibiotics Administered in High Concentrations on Primary Human Osteoblasts and Cell Lines. *Antimicrob. Agents Chemother.* **2007**, *51*, 54−63.

(19) Rams, T. E.; Degener, J. E.; Van Winkelhoff, A. J. Antibiotic Resistance in Human Peri-Implantitis Microbiota. *Clin. Oral Implants Res.* **2014**, *25*, 82−90.

(20) Mohanty, S.; Mishra, S.; Jena, P.; Jacob, B.; Sarkar, B.; Sonawane, A. An Investigation on the Antibacterial, Cytotoxic, and Antibiofilm Efficacy of Starch-Stabilized Silver Nanoparticles. *Nanomed. Nanotechnol., Biol. Med.* **2012**, *8*, 916−924.

(21) Hasan, J.; Webb, H. K.; Truong, V. K.; Pogodin, S.; Baulin, V. A.; Watson, G. S.; Watson, J. A.; Crawford, R. J.; Ivanova, E. P. Selective Bactericidal Activity of Nanopatterned Superhydrophobic Cicada Psaltoda Claripennis Wing Surfaces. *Appl. Microbiol. Biotechnol.* **2013**, *97*, 9257−9262.

(22) Ghilini, F.; Rodríguez González, M. C.; Miñán, A. G.; Pissinis, D.; Creus, A. H.; Salvarezza, R. C.; Schilardi, P. L. Highly Stabilized Nanoparticles on Poly- l -Lysine-Coated Oxidized Metals: A Versatile Platform with Enhanced Antimicrobial Activity. *ACS Appl. Mater. Interfaces* **2018**, *10*, 23657−23666.

(23) Pallavicini, P.; Dacarro, G.; Taglietti, A. Self-Assembled Monolayers of Silver Nanoparticles: From Intrinsic to Switchable Inorganic Antibacterial Surfaces. *Eur. J. Inorg. Chem.* **2018**, *2018*, 4846−4855.

(24) Oda, H.; Wakabayashi, H.; Yamauchi, K.; Abe, F. Lactoferrin and Bifidobacteria. *Biometals* **2014**, *27*, 915−922.

(25) Moreno-Expósito, L.; Illescas-Montes, R.; Melguizo-Rodríguez, L.; Ruiz, C.; Ramos-Torrecillas, J.; De Luna-bertos, E. Multifunctional Capacity and Therapeutic Potential of Lactoferrin. *Life Sci.* **2018**, *195*, 61−64.

(26) González-Chávez, S. A.; Arévalo-Gallegos, S.; Rascón-Cruz, Q. Lactoferrin: Structure, Function and Applications. *Int. J. Antimicrob. Agents* **2009**, *33*, 301.e1−301.e8.

(27) Cornish, J.; Palmano, K.; Callon, K. E.; Watson, M.; Lin, J. M.; Valenti, P.; Naot, D.; Grey, A. B.; Reid, I. R. Lactoferrin and Bone; Structure−Activity Relationships. *Biochem. Cell Biol.* **2006**, *84*, 297−302.

(28) Elzoghby, A. O.; Abdelmoneem, M. A.; Hassanin, I. A.; Abd Elwakil, M. M.; Elnaggar, M. A.; Mokhtar, S.; Fang, J. Y.; Elkhodairy, K. A. Lactoferrin, a Multi-Functional Glycoprotein: Active Therapeutic, Drug Nanocarrier & Targeting Ligand. *Biomaterials* **2020**, *263*, No. 120355.

(29) Kim, S. E.; Yun, Y. P.; Lee, J. Y.; Park, K.; Suh, D. H. Osteoblast Activity of MG-63 Cells Is Enhanced by Growth on a Lactoferrin-Immobilized Titanium Substrate. *Colloids Surf., B* **2014**, *123*, 191−198.

(30) Godoy-Gallardo, M.; Mas-Moruno, C.; Fernández-Calderón, M. C.; Pérez-Giraldo, C.; Manero, J. M.; Albericio, F.; Gil, F. J.; Rodríguez, D. Covalent Immobilization of HLf1-11 Peptide on a Titanium Surface Reduces Bacterial Adhesion and Biofilm Formation. *Acta Biomater.* **2014**, *10*, 3522−3534.

(31) McCafferty, E.; Wightman, J. An X-Ray Photoelectron Spectroscopy Sputter Profile Study of the Native Air-Formed Oxide Film on Titanium. *Appl. Surf. Sci.* **1999**, *143*, 92−100.

(32) Frank, A. J.; Cathcart, N.; Maly, K. E.; Kitaev, V. Synthesis of Silver Nanoprisms with Variable Size and Investigation of Their Optical Properties: A First-Year Undergraduate Experiment Exploring Plasmonic Nanoparticles. *J. Chem. Educ.* **2010**, *87*, 1098−1101.

(33) Pal, S.; Tak, Y. K.; Song, J. M. Does the Antibacterial Activity of Silver Nanoparticles Depend on the Shape of the Nanoparticle? A Study of the Gram-Negative Bacterium *Escherichia Coli*. *Appl. Environ. Microbiol.* **2007**, *73*, 1712−1720.

(34) Malaval, L.; Modrowski, D.; Gupta, A. K.; Aubin, J. E. Cellular Expression of Bone-related Proteins during in Vitro Osteogenesis in Rat Bone Marrow Stromal Cell Cultures. *J. Cell. Physiol.* **1994**, *158*, 555−572.

(35) Fernández, J. M.; Molinuevo, M. S.; Sedlinsky, C.; Schurman, L.; Cortizo, A. M.; McCarthy, A. D. Strontium Ranelate Prevents the Deleterious Action of Advanced Glycation Endproducts on Osteoblastic Cells via Calcium Channel Activation. *Eur. J. Pharmacol.* **2013**, *706*, 41−47.

(36) Bhutda, S.; Surve, M.; Anil, A.; Kamath, K.; Singh, N.; Modi, D.; Banerjee, A. Histochemical Staining of Collagen and Identification of Its Subtypes by Picrosirius Red Dye in Mouse Reproductive Tissues. *Bio-Protoc.* **2017**, *7*, No. 10.21769/BioProtoc.2592.

(37) Stanford, C. M.; Jacobson, P. A.; Eanes, E. D.; Lembke, L. A.; Midura, R. J. Rapidly Forming Apatitic Mineral in an Osteoblastic Cell Line (UMR 106-01 BSP). *J. Biol. Chem.* **1995**, *270*, 9420−9428.

(38) Anova, E.; La, D. *Análisis de Varianza de Un Factor: El Procedimiento ANOVA de Un Factor*. 251−266.

(39) Nagano-Takebe, F.; Miyakawa, H.; Nakazawa, F.; Endo, K. Inhibition of Initial Bacterial Adhesion to Titanium by Lactoferrin. *Eur. Cells Mater.* **2013**, *26*, No. 39.

(40) Cochis, A.; Ferraris, S.; Sorrentino, R.; Azzimonti, B.; Novara, C.; Geobaldo, F.; Truffa Giachet, F.; Vineis, C.; Varesano, A.; Sayed Abdelgeliel, A.; Spriano, S.; Rimondini, L. Silver-Doped Keratin Nanofibers Preserve a Titanium Surface from Biofilm Contamination and Favor Soft-Tissue Healing. *J. Mater. Chem. B* **2017**, *5*, 8366−8377.

(41) Agnihotri, S.; Mukherji, S.; Mukherji, S. Immobilized Silver Nanoparticles Enhance Contact Killing and Show Highest Efficacy: Elucidation of the Mechanism of Bactericidal Action of Silver. *Nanoscale* **2013**, *5*, 7328−7340.

(42) Yoshida, E.; Hayakawa, T. Adsorption Study of Pellicle Proteins to Gold, Silica and Titanium by Quartz Crystal Microbalance Method. *Dent. Mater. J.* **2013**, *32*, 883−887.

(43) Torrisi, T.; Scolaro, C. Nanoparticles Improving the Wetting Ability of Biological Liquids. *J. Thermodyn. Catal.* **2017**, *08*, 1−6.

(44) De Avila, E. D.; Lima, B. P.; Sekiya, T.; Torii, Y.; Ogawa, T.; Shi, W.; Lux, R. Effect of UV-Photofunctionalization on Oral Bacterial Attachment and Biofilm Formation to Titanium Implant Material. *Biomaterials* **2015**, *67*, 84−92.

(45) Godoy-Gallardo, M.; Mas-Moruno, C.; Yu, K.; Manero, J. M.; Gil, F. J.; Kizhakkedathu, J. N.; Rodriguez, D. Antibacterial Properties of HLf1-11 Peptide onto Titanium Surfaces: A Comparison Study between Silanization and Surface Initiated Polymerization. *Biomacromolecules* **2015**, *16*, 483−496.

(46) Li, J. H.; Shao, X. S.; Zhou, Q.; Li, M. Z.; Zhang, Q. Q. The Double Effects of Silver Nanoparticles on the PVDF Membrane:

https://doi.org/10.1021/acsabm.1c00613
ACS Appl. Bio Mater. XXXX, XXX, XXX−XXX

Surface Hydrophilicity and Antifouling Performance. *Appl. Surf. Sci.* **2013**, *265*, 663−670.

(47) Liu, J.; Hurt, R. H. Ion Release Kinetics and Particle Persistence in Aqueous Nano-Silver Colloids. *Environ. Sci. Technol.* **2010**, *44*, 2169−2175.

(48) Moore, S. A.; Anderson, B. F.; Groom, C. R.; Haridas, M.; Baker, E. N. Three-Dimensional Structure of Diferric Bovine Lactoferrin at 2.8 Å Resolution. *J. Mol. Biol.* **1997**, *274*, 222−236.

(49) Stoleru, E.; Zaharescu, T.; Hitruc, E. G.; Vesel, A.; Ioanid, E. G.; Coroaba, A.; Safrany, A.; Pricope, G.; Lungu, M.; Schick, C.; Vasile, C. Lactoferrin-Immobilized Surfaces onto Functionalized PLA Assisted by the Gamma-Rays and Nitrogen Plasma to Create Materials with Multifunctional Properties. *ACS Appl. Mater. Interfaces* **2016**, *8*, 31902−31915.

(50) Leaper, D.J.; Edmiston, C.E. World Health Organization: Global Guidelines on the Prevention of Surgical Site Infection. *J. Hosp. Infect.* **2017**, *95*, 135−136.

(51) Civantos, A.; Martínez-Campos, E.; Ramos, V.; Elvira, C.; Gallardo, A.; Abarrategi, A. Titanium Coatings and Surface Modifications: Toward Clinically Useful Bioactive Implants. *ACS Biomater. Sci. Eng.* **2017**, *3*, 1245−1261.

(52) Anselme, K.; Ploux, L.; Ponche, A. Cell/Material Interfaces: Influence of Surface Chemistry and Surface Topography on Cell Adhesion. *J. Adhes. Sci. Technol.* **2010**, *24*, 831−852.

(53) Wei, J.; Yoshinari, M.; Takemoto, S.; Hattori, M.; Kawada, E.; Liu, B.; Oda, Y. Adhesion of Mouse Fibroblasts on Hexamethyldisiloxane Surfaces with Wide Range of Wettability. *J. Biomed. Mater. Res., Part B* **2007**, *81B*, 66−75.

(54) Zelzer, M.; Majani, R.; Bradley, J. W.; Rose, F. R. A. J.; Davies, M. C.; Alexander, M. R. Investigation of Cell-Surface Interactions Using Chemical Gradients Formed from Plasma Polymers. *Biomaterials* **2008**, *29*, 172−184.

(55) Lim, J. Y.; Liu, X.; Vogler, E. A.; Donahue, H. J. Systematic Variation in Osteoblast Adhesion and Phenotype with Substratum Surface Characteristics. *J. Biomed. Mater. Res., Part A* **2004**, *68A*, 504−512.

(56) Cai, S.; Wu, C.; Yang, W.; Liang, W.; Yu, H.; Liu, L. Recent Advance in Surface Modification for Regulating Cell Adhesion and Behaviors. *Nanotechnol. Rev.* **2020**, *9*, 971−989.

(57) Zareidoost, A.; Yousefpour, M.; Ghaseme, B.; Amanzadeh, A. The Relationship of Surface Roughness and Cell Response of Chemical Surface Modification of Titanium. *J. Mater. Sci.: Mater. Med.* **2012**, *23*, 1479−1488.

(58) Icriverzi, M.; Bonciu, A.; Rusen, L.; Sima, L. E.; Brajnicov, S.; Cimpean, A.; Evans, R. W.; Dinca, V.; Roseanu, A. Human Mesenchymal Stem Cell Response to Lactoferrin-Based Composite Coatings. *Materials (Basel)* **2019**, *12*, No. 20.

(59) Constantinescu, C.; Palla-Papavlu, A.; Rotaru, A.; Florian, P.; Chelu, F.; Icriverzi, M.; Nedelcea, A.; Dinca, V.; Roseanu, A.; Dinescu, M. Multifunctional Thin Films of Lactoferrin for Biochemical Use Deposited by MAPLE Technique. *Appl. Surf. Sci.* **2009**, *255*, 5491−5495.

(60) Shen, T.; Yang, W.; Shen, X.; Chen, W.; Tao, B.; Yang, X.; Yuan, J.; Liu, P.; Cai, K. Polydopamine-Assisted Hydroxyapatite and Lactoferrin Multilayer on Titanium for Regulating Bone Balance and Enhancing Antibacterial Property. *ACS Biomater. Sci. Eng.* **2018**, *4*, 3211−3223.

(61) Zhang, X. F.; Shen, W.; Gurunathan, S. Silver Nanoparticle-Mediated Cellular Responses in Various Cell Lines: An in Vitro Model. *Int. J. Mol. Sci.* **2016**, *17*, No. 1603.

(62) Pauksch, L.; Hartmann, S.; Rohnke, M.; Szalay, G.; Alt, V.; Schnettler, R.; Lips, K. S. Biocompatibility of Silver Nanoparticles and Silver Ions in Primary Human Mesenchymal Stem Cells and Osteoblasts. *Acta Biomater.* **2014**, *10*, 439−449.

(63) Kzhyshkowska, J.; Gudima, A.; Riabov, V.; Dollinger, C.; Lavalle, P.; Vrana, N. E. Macrophage Responses to Implants: Prospects for Personalized Medicine. *J. Leukocyte Biol.* **2015**, *98*, 953−962.

(64) Vogel, D. Y. S.; Glim, J. E.; Stavenuiter, A. W. D.; Breur, M.; Heijnen, P.; Amor, S.; Dijkstra, C. D.; Beelen, R. H. J. Human Macrophage Polarization in Vitro: Maturation and Activation Methods Compared. *Immunobiology* **2014**, *219*, 695−703.

(65) Blair, H. C.; Larrouture, Q. C.; Li, Y.; Lin, H.; Beer-Stoltz, D.; Liu, L.; Tuan, R. S.; Robinson, L. J.; Schlesinger, P. H.; Nelson, D. J. Osteoblast Differentiation and Bone Matrix Formation In Vivo and In Vitro. *Tissue Eng., Part B* **2017**, *23*, 268−280.

(66) Kim, S. E.; Yun, Y. P.; Shim, K. S.; Park, K.; Choi, S. W.; Suh, D. H. Effect of Lactoferrin-Impregnated Porous Poly(Lactide-Co-Glycolide) (PLGA) Microspheres on Osteogenic Differentiation of Rabbit Adipose-Derived Stem Cells (RADSCs). *Colloids Surf., B* **2014**, *122*, 457−464.

(67) Kim, S. E.; Song, S. H.; Yun, Y. P.; Choi, B. J.; Kwon, I. K.; Bae, M. S.; Moon, H. J.; Kwon, Y. D. The Effect of Immobilization of Heparin and Bone Morphogenic Protein-2 (BMP-2) to Titanium Surfaces on Inflammation and Osteoblast Function. *Biomaterials* **2011**, *32*, 366−373.

(68) Montesi, M.; Panseri, S.; Iafisco, M.; Adamiano, A.; Tampieri, A. Effect of Hydroxyapatite Nanocrystals Functionalized with Lactoferrin in Osteogenic Differentiation of Mesenchymal Stem Cells. *J. Biomed. Mater. Res., Part A* **2015**, *103*, 224−234.

(69) Gittens, R. A.; McLachlan, T.; Olivares-Navarrete, R.; Cai, Y.; Berner, S.; Tannenbaum, R.; Schwartz, Z.; Sandhage, K. H.; Boyan, B. D. The Effects of Combined Micron-/Submicron-Scale Surface Roughness and Nanoscale Features on Cell Proliferation and Differentiation. *Biomaterials* **2011**, *32*, 3395−3403.

https://doi.org/10.1021/acsabm.1c00613
ACS Appl. Bio Mater. XXXX, XXX, XXX−XXX